J|A|C|S ARTICLES

Published on Web 03/20/2009

Formation of Monodisperse FePt Alloy Nanocrystals Using Air-Stable Precursors: Fatty Acids as Alloying Mediator and Reductant for Fe^{3+} Precursors

Fei Zhao, Michael Rutherford, Susan Y. Grisham, and Xiaogang Peng*

Department of Chemistry and Biochemistry, University of Arkansas, Fayetteville, Arkansas 72701

Received January 12, 2009; E-mail: xpeng@uark.edu

Abstract: High quality FePt nanocrystals were synthesized by a simple and high performance synthetic method in a hydrocarbon solvent. Instead of a toxic and dangerous $Fe(CO)_5$ precursor, air-stable and generic inorganic and organic iron salts were used as the iron precursors. Fatty acid molecules were identified as both efficient reducing reagents for the Fe^{3+} precursors and as an alloying mediator. The alloying process occurred in a two-step fashion. The Pt nanocrystal seeds initially formed at relatively low temperatures, with the need to be stabilized by a small amount of amines. Conversely, the final FePt nanocrystals could be stabilized with fatty acids as the main ligands. The mechanisms revealed here not only help to understand the formation of alloy nanocrystals but also shed new light on the formation of transition metal oxide nanocrystals using metal fatty acid salts as the precursors.

Introduction

Colloidal magnetic nanocrystals are of great interest in biomedical imaging, drug delivery, sensing, memory devices, etc.[1−8] Magnetic nanocrystals can be classified into three different classes, namely metal oxides, metal alloys, and metallic. Metal oxides are normally not very strong in magnetic properties, but they are typically stable under ambient conditions. Conversely, metallic ones are magnetically strong but typically unstable. Metal alloys, such as FePt and CoPt ones, are reasonably good on both magnetic strength and stability.[9−11] For instance, in comparison to the coercivity of the corresponding magnetic oxides, Fe_3O_4 and γ-Fe_2O_3, FePt possesses significantly higher values, either approximately 2 orders of magnitude higher in *fct* structure or 1 order of magnitude higher in *fcc* structure.[1,12,13] In terms of stability, FePt nanocrystals are found to be even more stable than iron oxides. Alloy nanocrystals are not only interesting in the field of magnetic nanomaterials but also of importance in catalysis, bandgap tuning in semiconductor nanocrystals, etc.[14−16] Therefore, fundamental investigations on alloying in the nanometer size regime are of general importance in materials chemistry.

However, synthesis of alloy nanocrystals requires an additional controlling parameter in addition to size and shape control for the nanocrystals with simple and fixed compositions. In typical alloy systems the phases of the pure components, such as pure metal Fe and Pt phases associated with the FePt alloy, are usually stable phases under the given conditions. A question remains in the nanometer size regime: how does the alloying of Fe and Pt occur? For alloys involving transition metals, their corresponding oxides (such as iron oxide) may also exist in many different stable phases.[17] How can one avoid the formation of the transition metal oxides?

(1) Sun, S. H.; Murray, C. B.; Weller, D.; Folks, L.; Moser, A. *Science* **2000**, *287*, 1989–1992.
(2) Hafeli, U.; Schutt, W.; Teller, J.; Zborowski, M. *Scientific and Clinical Applications of magnetic Carriers*; Plenum Press: New York, 1997.
(3) Zeng, H.; Li, J.; Liu, J. P.; Wang, Z. L.; Sun, S. H. *Nature* **2002**, *420*, 395–398.
(4) Pankhurst, Q. A.; Connolly, J.; Jones, S. K.; Dobson, J. *J. Phys. D: Appl. Phys.* **2003**, *36*, R167−R181.
(5) Teng, X. W.; Yang, H. *J. Am. Chem. Soc.* **2003**, *125*, 14559–14563.
(6) Seo, W. S.; Lee, J. H.; Sun, X. M.; Suzuki, Y.; Mann, D.; Liu, Z.; Terashima, M.; Yang, P. C.; McConnell, M. V.; Nishimura, D. G.; Dai, H. J. *Nat. Mater.* **2006**, *5*, 971–976.
(7) Tromsdorf, U. I.; Bigall, N. C.; Kaul, M. G.; Bruns, O. T.; Nikolic, M. S.; Mollwitz, B.; Sperling, R. A.; Reimer, R.; Hohenberg, H.; Parak, W. J.; Forster, S.; Beisiegel, U.; Adam, G.; Weller, H. *Nano Lett.* **2007**, *7*, 2422–2427.
(8) Laurent, S.; Forge, D.; Port, M.; Roch, A.; Robic, C.; Elst, L. V.; Muller, R. N. *Chem. Rev.* **2008**, *108*, 2064–2110.
(9) Yiu, E. Y. L.; Fang, D. T. S.; Chu, F. C. S.; Chow, T. W. *J. Dent.* **2004**, *32*, 423–429.
(10) Antoniak, C.; Lindner, J.; Spasova, M.; Sudfeld, D.; Acet, M.; Farle, M.; Fauth, K.; Wiedwald, U.; Boyen, H. G.; Ziemann, P.; Wilhelm, F.; Rogalev, A.; Sun, S. H. *Phys. Rev. Lett.* **2006**, *97*, 4.
(11) Gebert, A.; Roth, S.; Gopalan, R.; Kundig, A. A.; Schultz, L. *J. Alloy Compd.* **2007**, *436*, 309–312.
(12) Varanda, L. C.; Jafelicci, M. *J. Am. Chem. Soc.* **2006**, *128*, 11062–11066.
(13) Rutledge, R. D.; Morris, W. H.; Wellons, M. S.; Gai, Z.; Shen, J.; Bentley, J.; Wittig, J. E.; Lukehart, C. M. *J. Am. Chem. Soc.* **2006**, *128*, 14210–14211.
(14) Chen, W.; Kim, J. M.; Sun, S. H.; Chen, S. W. *Langmuir* **2007**, *23*, 11303–11310.
(15) Antolini, E.; Salgado, J. R. C.; Gonzalez, E. R. *J. Power Sources* **2006**, *160*, 957–968.
(16) Zhong, X. H.; Han, M. Y.; Dong, Z. L.; White, T. J.; Knoll, W. *J. Am. Chem. Soc.* **2003**, *125*, 8589–8594.
(17) Shtykova, E. V.; Huang, X. L.; Remmes, N.; Baxter, D.; Stein, B.; Dragnea, B.; Svergun, D. I.; Bronstein, L. M. *J. Phys. Chem. C* **2007**, *111*, 18078–18086.
(18) Howard, L. E. M.; Nguyen, H. L.; Giblin, S. R.; Tanner, B. K.; Terry, I.; Hughes, A. K.; Evans, J. S. O. *J. Am. Chem. Soc.* **2005**, *127*, 10140–10141.
(19) Sun, S. H. *Adv. Mater.* **2006**, *18*, 393–403.
(20) Chen, M.; Kim, J.; Liu, J. P.; Fan, H. Y.; Sun, S. H. *J. Am. Chem. Soc.* **2006**, *128*, 7132–7133.

10.1021/ja900202t CCC: $40.75

Provided the importance of metal alloy magnetic nanocrystals, especially FePt ones, their synthesis has been widely studied in the field.[1,18−20] The most successful methods, however, were based on the use of toxic and dangerous transition metal carbonyl complexes, such as $Fe(CO)_5$. With $Fe(CO)_5$ as the iron precursor, various reports show that it is possible to produce nearly monodisperse FePt nanocrystals in the size range between 2 and 15 nm.[21,22] However, because of environmental concerns and ease for control, the general trend in the field of synthesis of colloidal nanocrystals has been moving away from toxic, unstable, and dangerous organometallic precursors to air-stable and less toxic ones, namely "greener approaches".[23] For Pt, $Pt(acac)_2$ is acceptable. Iron fatty acid salts and common inorganic iron salts that are soluble in organic solvents with simple ligands should be the ideal choices for the iron precursors.[24−27] However, without additional reducing reagents, control of the size distribution and composition has remained a general challenge.

There are some indications for using iron fatty acid salts as the precursors without using reducing reagents. In the formation of high quality Fe_3O_4 nanocrystals, it was typically accomplished by heating iron (Fe^{3+}) fatty acid salts in a noncoordinating solvent, such as ocadecene (ODE). Obviously, some of the Fe^{3+} ions are reduced in such a scheme although no additional reducing reagents were added.[28−30] Mass spectroscopy measurements on such systems revealed the formation of CO_2 gas, indicating that fatty acids might be reducing reagents in this specific case.[31] Finally, formation of FePt nanocrystals using iron fatty acid salts without reducing reagents showed some degree of success.[27,32,33]

This report will focus on identifying the role of fatty acids as both the reductants for Fe^{3+} fatty acid salt precursors and the alloying mediator for the FePt alloy system. The mechanism studies in this report will be more on the chemical changes involved, instead of growth kinetics of the nanocrystals typically investigated in the past.[34,35]

Results

The basic reaction system included iron fatty acid salts as the iron precursor, $Pt(acac)_2$ as the platinum precursor, octadecene (ODE) or tetracosane (TCA) as the solvent, and fatty amines and fatty acids as the ligands. It was found that the double bond of ODE underwent some chemical reactions probably due to the Pt nanocrystals.[36] Although this fact did not affect the formation of the alloy nanocrystals, to simplify the mechanism studies, long chain alkanes were used as the solvent. Fatty amines were found to be essential as ligands for the Pt nanocrystals formed in the early stages of the reaction. The role of the fatty acids and their corresponding Fe^{3+} salt, typically stearic acid (HSt) and iron stearate ($Fe(St)_3$),seemed to be quite diverse which constitutes the major part of this report. Some preliminary studies were carried out on those iron inorganic salts, such as $FeCl_3$ and $Fe(NO_3)_3$ that are soluble in the hydrocarbon solvents by mixing with fatty acids (Figure 1). The mechanisms for the reactions using inorganic salts will be reported separately due to the complication arising from the counterions of the iron precursors. Figure 1 briefly summarizes the reaction system discussed here.

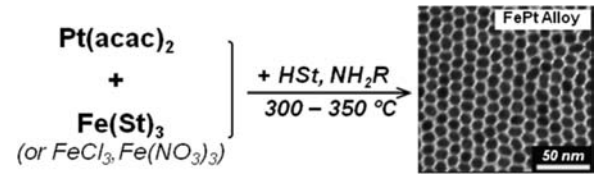

Figure 1. Illustration of the formation of FePt alloy. The mechanisms for the reactions using the inorganic iron salts will be reported separately.

The general structure characterization, including size, size distribution, and crystal structure, of the as-synthesized nanocrystals was performed for the samples without any size sorting. The TEM images (top panel, Figure 2) illustrate six examples of the nearly monodisperse nanocrystals grown by the synthetic scheme shown in Figure 1. The corresponding HRTEM images of the samples are shown in the bottom panel, which revealed the single crystalline nature of the nanocrystals. The lattice spacings in the HRTEM images (see examples in Figure 2, bottom) were found to be consistent with that of *fcc* (face-centered cubic) alloy FePt.

To further confirm the crystal structure and overall phase purity, the nanocrystals with different sizes were examined using XRD. As shown in Figure 3 (top), all samples were found to be consistent with the expected diffraction pattern of the *fcc* FePt structures. Neither iron oxide nor iron metal phases were observed. From the peak width of the strongest peak, (111), the domain size of the particles was estimated using the Sherrer equation, which matched well with the particle sizes determined by TEM.

The magnetization of the nanocrystals shown in Figure 2 was measured (Figure 3, bottom). When the size of these nearly monodipserse nanocrystals reached 11 nm, its magnetization value ($H = 4500$ Oe) was found to be close to the saturated value bulk for the FePt alloy in *fcc* structure of 1140 emu/cm^3.[37] As the size of the nanocrystals decreased, the magnetization decreased substantially and was found to be inversely correlated with the surface to volume atom ratio of the nanocrystals (Figure 2, bottom). These facts confirmed the magnetic feature of the resulting nanocrystals and the well-known surface destruction

(21) Chen, M.; Liu, J. P.; Sun, S. H. *J. Am. Chem. Soc.* **2004**, *126*, 8394–8395.
(22) Nandwana, V.; Elkins, K. E.; Poudyal, N.; Chaubey, G. S.; Yano, K.; Liu, J. P. *J. Phys. Chem. C* **2007**, *111*, 4185–4189.
(23) Peng, X. G. *Chem.—Eur. J.* **2002**, *8*, 335–339.
(24) Iwaki, T.; Kakihara, Y.; Toda, T.; Abdullah, M.; Okuyama, K. *J. Appl. Phys.* **2003**, *94*, 6807–6811.
(25) Harpeness, R.; Gedanken, A. *J. Mater. Chem.* **2005**, *15*, 698–702.
(26) Saita, S.; Maenosono, S. *Chem. Mater.* **2005**, *17*, 3705–3710.
(27) Saita, S.; Maenosono, S. *Chem. Mater.* **2005**, *17*, 6624–6634.
(28) Jana, N. R.; Chen, Y. F.; Peng, X. G. *Chem. Mater.* **2004**, *16*, 3931–3935.
(29) Park, J.; An, K. J.; Hwang, Y. S.; Park, J. G.; Noh, H. J.; Kim, J. Y.; Park, J. H.; Hwang, N. M.; Hyeon, T. *Nat. Mater.* **2004**, *3*, 891–895.
(30) Yu, W. W.; Falkner, J. C.; Yavuz, C. T.; Colvin, V. L. *Chem. Commun.* **2004**, 2306–2307.
(31) Kwon, S. G.; Piao, Y.; Park, J.; Angappane, S.; Jo, Y.; Hwang, N. M.; Park, J. G.; Hyeon, T. *J. Am. Chem. Soc.* **2007**, *129*, 12571–12584.
(32) Sun, S. H.; Anders, S.; Thomson, T.; Baglin, J. E. E.; Toney, M. F.; Hamann, H. F.; Murray, C. B.; Terris, B. D. *J. Phys. Chem. B* **2003**, *107*, 5419–5425.
(33) Nakaya, M.; Kanehara, M.; Teranishi, T. *Langmuir* **2006**, *22*, 3485–3487.
(34) Peng, X. G.; Thessing, J. *Semiconductor Nanocrystals and Silicate Naoparticles*; Springer-Verlag Berlin: Berlin, 2005; Vol. 118, pp 79−119.
(35) Shevchenko, E. V.; Talapin, D. V.; Schnablegger, H.; Kornowski, A.; Festin, O.; Svedlindh, P.; Haase, M.; Weller, H. *J. Am. Chem. Soc.* **2003**, *125*, 9090–9101.
(36) Lewis, L. N.; Sy, K. G.; Donahue, P. E. *J. Organomet. Chem.* **1992**, *427*, 165–172.
(37) Weller, D.; Moser, A.; Folks, L.; Best, M. E.; Lee, W.; Toney, M. F.; Schwickert, M.; Thiele, J. U.; Doerner, M. F. *IEEE Trans. Magn.* **2000**, *36*, 10–15.

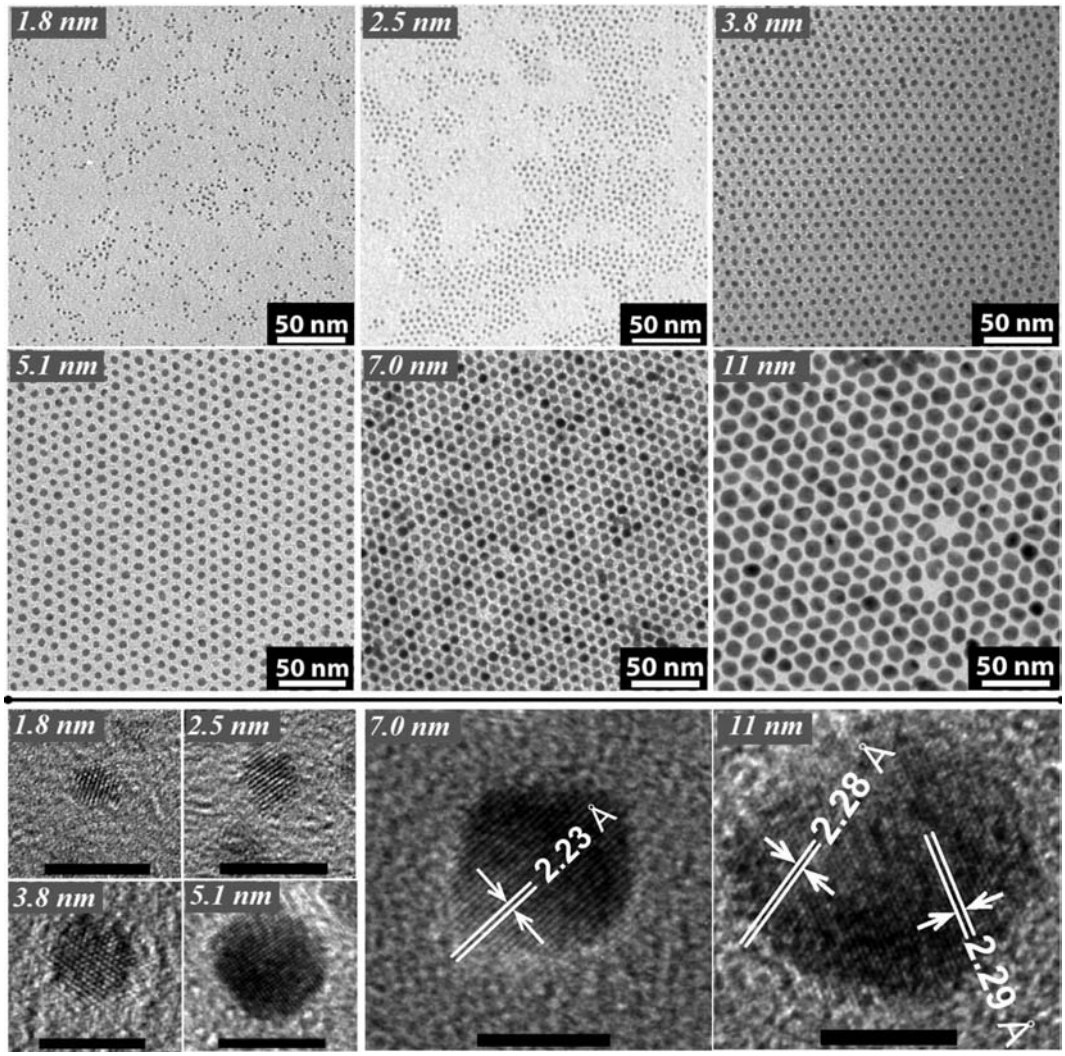

Figure 2. Top panel: TEM images of the as-prepared FePt alloy nanocrystals. Bottom panel: the corresponding HRTEM images (Scale bar for HRTEM: 5 nm).

of the magnetic ordering in nanocrystals.[38] These results imply that the nanocrystals shown in Figure 2 were consistent with the *fcc* PtFe alloy nanocrystals, instead of pure Pt nanocrystals.

A large excess of fatty acids were found to yield FePt alloy nanocrystals without complications of iron metal and iron oxides when iron fatty acid salts were used as the precursors in long chain hydrocarbon solvents, such as tetracosane (TCA) and ocadecene (ODE). For a specific reaction (Figure 4), $Fe(St)_3$, $Pt(acac)_2$, HSt, and octadecylamine (ODA) were mixed with molar ratios of 1:1:8:5 in TCA and heated to 350 °C at 10 °C/min. Though a systematic variation of the fatty acid concentration was studied, this reaction is a representative example of the reactions with a large excess of fatty acids.

When the reaction temperature was below ~270 °C, TEM observations revealed small particles, ~1.5 nm in size (Figure 4, left panel). The corresponding EDX spectrum identified the existence of the Pt element and no existence of any iron element in the purified sample. The electron diffraction pattern indicated that the Pt nanocrystals were in *fcc* structure. Consistent with the formation of Pt nanocrystals, the FTIR spectrum revealed that the vibrational bands at 1523 and 1558 cm^{-1}, associated with $Pt(acac)_2$, disappeared almost completely when the temperature reached 250 °C (Figure 4, right panel).

Figure 4 (middle panel) shows the TEM image along with the associated EDX spectrum of FePt alloy nanocrystals obtained by heating the typical reaction to 350 °C. In comparison to the Pt nanocrystals formed at lower temperatures, these nanocrystals were substantially larger, ~1.9 nm on average. This size increase from 1.5 to 1.9 nm is approximately equivalent to doubling the volume of the nanocrystals. EDX measurements demonstrated the existence of the Fe element in the purified nanocrystal sample (Figure 4, middle panel), instead of only the Pt element observed at lower temperatures (Figure 4, left panel). The Fe/Pt ratio for this specific sample was found to be close to 1:1 by EDX calculations, which matched the volume increase observed by TEM. Electron diffraction and X-ray diffraction patterns of the nanocrystals obtained at 350 °C showed no existence of pure Fe metal and iron oxide phases. These nanocrystals also showed expected magnetic properties as discussed above. All of these results supported the formation of phase-pure alloy nanocrystals without the complication of pure iron and iron oxides.

Along with the formation of FePt alloy nanocrystals, the broad FTIR peak around 1713 cm^{-1} that was ascribed to ν(COOH)

(38) Sun, S. H.; Zeng, H.; Robinson, D. B.; Raoux, S.; Rice, P. M.; Wang, S. X.; Li, G. X. *J. Am. Chem. Soc.* **2004**, *126*, 273–279.

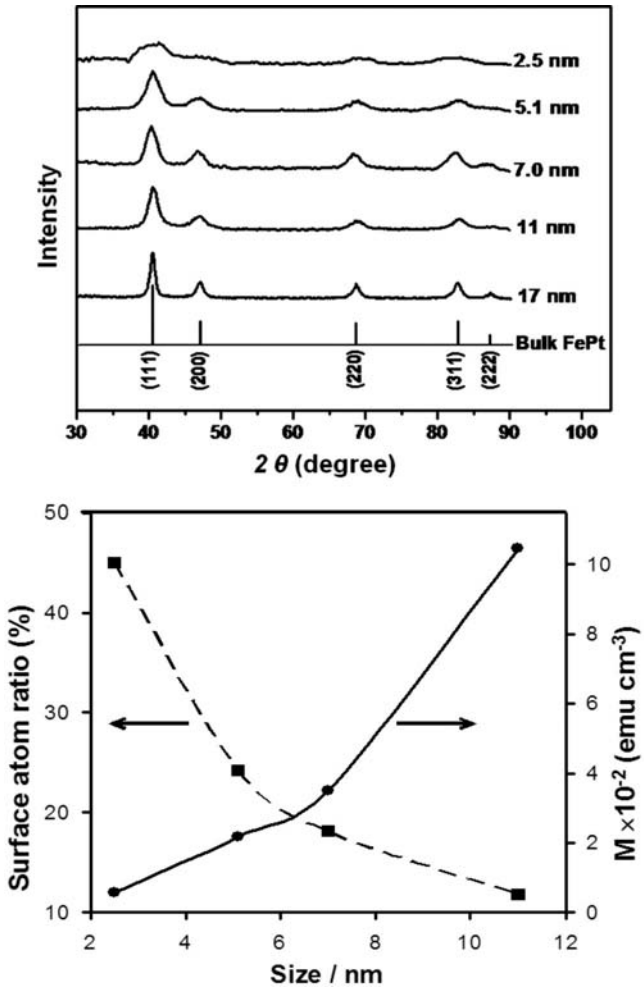

Figure 3. Top: Powder XRD patterns of the FePt NCs with different size ranges. Bottom: Magnetization (M) measured in an external magnetic field ($H = 4500$ Oe) and surface to volume atom ratio of the nanocrystals with different sizes.

in the liquid state[39] (see Figure S1) disappeared finally. The peak at 1530 cm^{-1}, associated with the asymmetry vibration of COO^-, shifted to 1572 cm^{-1} at 310 °C and then disappeared at 350 °C. These results were consistent with the conclusion drawn in the last paragraph that all Fe components were found in the form of FePt nanocrystals at 350 °C, instead of being in the form of $Fe(St)_3$.

The appearance of the IR peak at ~1639 cm^{-1} ascribed to the amide carbonyl vibration and disappearance of the peak at 1605 cm^{-1} associated with the $-NH_2$ deformational vibration in Figure 4 (right panel, from 220 to 250 °C) imply the formation of amide in the current reaction system.[39] This conclusion was further supported by the changing of the N−H stretching vibration in the Supporting Information (Figure S2). Interestingly, the formation of an amide was first detected slightly at 250 °C and was prevalent by 310 °C. According to the existing literature, fatty amines can react readily with transition metal fatty acid salts to form metal oxides and amides.[28] In this case, amines were considered as the activation reagents for the formation of oxides. However, as described above, no iron oxide phases were detected in this reaction at any stage. In comparison, the reactions without a large excess of fatty acids showed clear signs for the formation of iron oxides (see Figure S3). This indicates that the free fatty acids dissolved the iron oxide immediately after their formation. It should be pointed out that a similar reaction was actually observed in other metal oxide nanocrystal systems, such as ZnO, MnO, and In_2O_3 as well.[28,40,41]

The FTIR spectrum at 350 °C in Figure 4 shows a pair of twin peaks at 1699 and 1705 cm^{-1}, which is consistent with the stretching vibrations of the carbonyl group in ketones.[39] Further evidence confirming the formation of ketones will be given in the following subsection. These twin peaks, however, were absent in the FTIR spectra below 300 °C when the nanocrystals were pure Pt ones. This means that the generation of the ketone and the formation of FePt alloy nanocrystals occurred simultaneously. In comparison, the formation of amide discussed in the above paragraph was prior to the formation of the FePt alloy nanocrystals.

Formation of ketone and FePt nanocrystals from free fatty acids and iron stearate imply the presence of redox reactions in the current system. To further identify the chemical changes involved in this critical step, reduction of Fe^{3+}, reactions without any $Pt(acac)_2$ added were studied and the results are given in the following subsection.

Thermal treatment of $Fe(St)_3$ with the presence of HSt was carried out in TCA under Ar flow in the same temperature range for the formation of FePt alloy nanocrystals described in the above subsection. In comparison to the reaction associated with Figure 4, all reactions discussed in this subsection, $Pt(acac)_2$ and amines were excluded to isolate the redox processes between Fe^{3+} and fatty acids. There were some clear distinctions among the reactions with a different concentration of HSt.

Reactions without (or with a small amount of) HSt were found to yield iron oxide nanocrystals, mostly Fe_3O_4 ones.[28−30] As shown in Figure S4, FTIR measurements revealed the formation of free HSt at temperatures below 305 °C, indicating a hydrolysis process as observed for the formation of MnO and In_2O_3 nanocrystals.[40,41] However, when the temperatures reached 330 °C and above, the broad peak of the free fatty acid gradually disappeared and the appearance of the twin peaks associated with ketone became apparent (Figure S4). This means that even in the case of traditional synthetic schemes for Fe_3O_4 nanocrystals, formation of a ketone could also be a possible reaction pathway. This was considered to be reasonable, provided that the oxidation states of the iron component in Fe_3O_4 were a mixture of Fe^{2+} and Fe^{3+}, though the starting iron precursor was composed of Fe^{3+} only.

When the thermal treatment of $Fe(St)_3$ was carried out in pure HSt without TCA, the intensity of asymmetric vibration attributed to COO^- (1527 and 1590 cm^{-1}) did not decrease until the FTIR signals associated with HSt, namely the broad carbonyl vibration peak at ~1703 cm^{-1} and the broad C−O−H vibration band at 1296 cm^{-1}, started to decrease (Figure S5). It is worth noting that, even with temperatures up to 350 °C for 25 min, the carboxylate vibration peaks still remained more or less the same. This strongly supports the hypothesis that an excess amount of free HSt would dissolve the iron oxide and pure iron formed in the temperature range up to the limit of the current reaction system, 350 °C. As a result, the net result was the gradual disappearance of free HSt and a constant concentration

(39) Bellamy, L. J. *The Infra-Red Spectra of Complex Molecules*, 3rd ed.; Halsted: New York, 1975.
(40) Narayanaswamy, A.; Xu, H. F.; Pradhan, N.; Kim, M.; Peng, X. G. *J. Am. Chem. Soc.* **2006**, *128*, 10310–10319.
(41) Chen, Y. F.; Johnson, E.; Peng, X. G. *J. Am. Chem. Soc.* **2007**, *129*, 10937–10947.

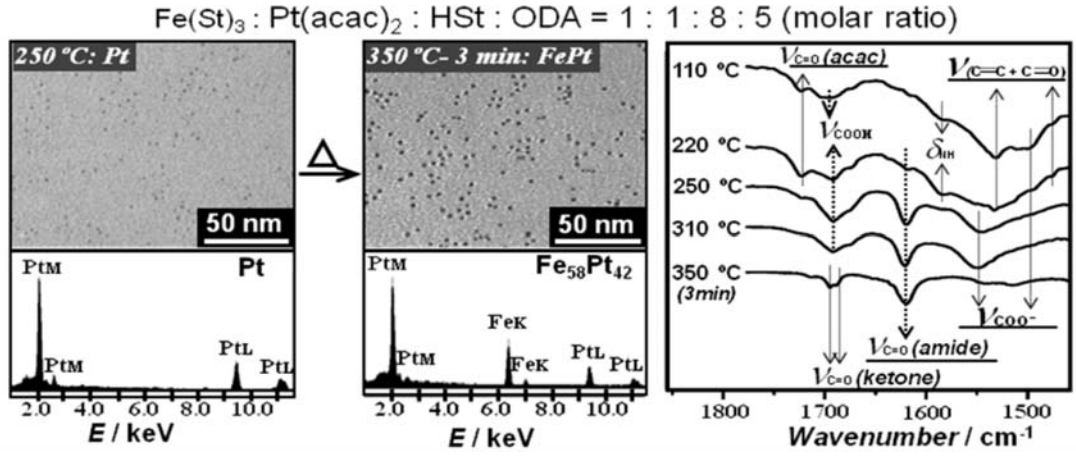

Figure 4. TEM, EDX, and FT-IR results of the reaction with sufficient acid as ligands.

of $Fe(St)_3$. At the end of the thermal treatment under this condition, all carboxylate and carboxylic acid vibrations disappeared. Instead, the twin peaks associated with ketones became evident. It should be pointed out that the inorganic products identified by electron diffraction were found to be a mixture of pure iron and iron oxide, which also supported the hypothesis.

The thermal behavior of $Fe(St)_3$ with an excess of HSt using TCA as the solvent—but not neat HSt as discussed in the above paragraph—was studied under the same reaction conditions as those for the reaction shown in Figure 4 without the presence of $Pt(acac)_2$. Figure 5 (top) shows the FTIR spectra of the reaction mixtures at different temperatures, both vapor phase and liquid phase mixtures. The completion of the reaction, indicated by the complete disappearance of carboxyalte and carboxylic vibrations and maximum strength of the twin peaks of the ketones, occurred after ~25 min at 350 °C, which was significantly faster than the reaction in neat HSt (see discussions in the above paragraph and Figure S5). This again supported that the pure iron and iron oxide would be dissolved by the excess free fatty acids. It should also be noted that, without the preformed Pt nanocrystals, the depletion of iron stearate was much slower (comparing the FTIR spectra in Figure 4 and the liquid aliquots spectra in Figure 5). This is very consistent with the formation of FePt nanocrystals due to the outstanding stability of FePt nanocrystals under acidic conditions.

CO_2 was detected in the vapor phase mixture by FTIR (Figure 5, top left) and $BaCO_3$ formation by bubbling the reaction vapor into a $Ba(OH)_2$ solution. The evolution of CO_2 was enhanced as the reaction temperature increased, and it stopped after the reaction was maintained at 350 °C for 45 min. The TGA spectrum of neat $Fe(St)_3$ showed that the precursor began to lose mass at 200 °C and completed at ~400 °C (shown in Figure S6), which is approximately consistent with the FTIR results discussed here. It is interesting that CO_2 started to be detectable at ~210 °C, which means that the reductive decomposition of $Fe(St)_3$ occurred at a rather low reaction temperature. This is consistent with the formation of Fe_3O_4 nanocrystals at 300 °C or below.[30] Another gas phase side product was found to be water vapor which was identified by condensation of the vapor.

The structures of the organic side products generated by the redox reactions between Fe^{3+} and fatty acids were further identified by ^1H NMR, ^{13}C NMR, and two-dimensional (2D) NMR (Figure 5c) coupled with FTIR. To make the assignment easier, the detailed analysis was carried out for the reaction in neat HSt without TCA as the solvent. The ^1H NMR spectrum of the organic side products suggested the existence of a β-CH_2 proton to the C═O group (Figure S7) but could not distinguish ketone from acid. The ^{13}C NMR spectrum (Figure 5, bottom), however, shows a peak at 211.8 ppm, which is consistent with a ketone chemical shift. As shown in the Supporting Information (Figure S7), the carbonyl group of HSt shows its ^{13}C NMR peak significantly upfield, at 180.1 ppm. 2D HMQC NMR (Figure 5 bottom, inset) further confirmed this assignment. The strong signal located at 2.38 ppm (^1H NMR) was associated with the 42.8 ppm peak in ^{13}C NMR spectrum, which confirms the existence of a β-CH_2 beside the C═O group from a ketone. For stearic acid, the β-CH_2 is located at 32.2 ppm in the ^{13}C NMR spectrum and 2.35 ppm in the ^1H NMR spectrum. The FTIR results also supported the formation of a ketone, instead of carboxylic acid. Although the IR peaks for carbonyl vibrations for ketones and acids were at similar wavenumbers, at ~1700 cm^{-1} (Figure 5a), the resulting organic side products did not show the characteristic broadband of coupled C−O and O−H vibrations at 1295 cm^{-1} for the −COOH group (comparing the FTIR spectrum at the very top with the one at the very bottom in Figure 5a).

The integration values of the ^1H NMR spectra for the purified organic side products (Supporting Information) matched what was expected for the ketone formed by two HSt molecules (with one molecule of water and CO_2 as the other products). However, the total integration of ^1H NMR of the raw organic product during the decomposition of $Fe(St)_3$ in neat HSt (Figure S7) suggests that ketone was not the major product, which accounted for only ~25% of the organic products using $-CH_3$ as the reference. There was ~20% of alkenes, both −CH═CH− and $-CH=CH_2$ types. The rest should be saturated alkanes, ~55%. The detailed analysis is provided in the Supporting Information (Table S1).

The thermal decomposition process of $Pt(acac)_2$ was also monitored by FT-IR and TEM to assist the clarification of the chemical changes associated with $Fe(St)_3$. As shown in Figure S8, The IR spectra showed that the $Pt(acac)_2$ began to decompose at ~200 °C and completed at ~250 °C, which is consistent with the illustration in Figure 4 (top panel and the text related). Meanwhile, the solution turned black in this temperature range, indicating the decomposition of precursors. When HSt or another long chain fatty acid was added into the system, the starting decomposition temperature decreased to 170 °C, while the existence of amine did not affect the decomposition temperature significantly.

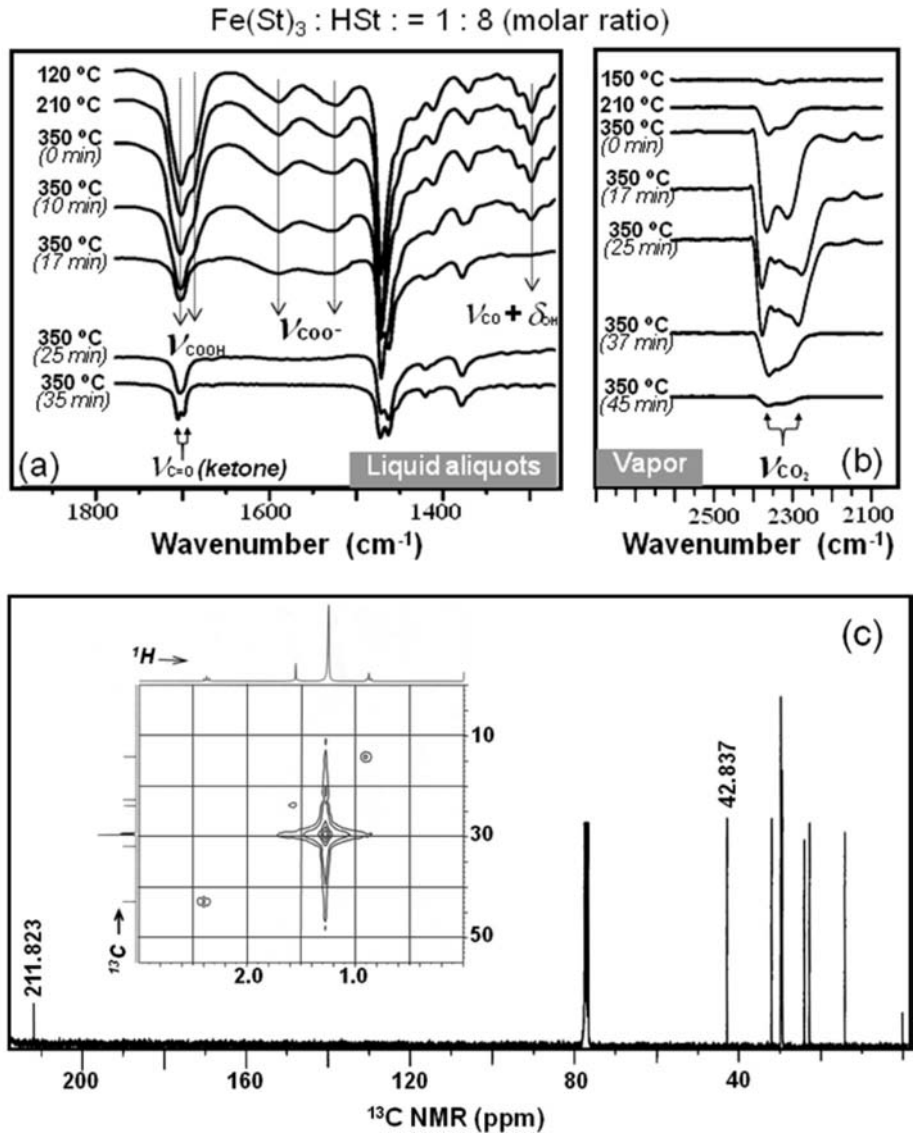

Figure 5. Top: FT-IR spectra of liquid aliquots (a) and vapor aliquots (b) recorded for the thermal decomposition of $Fe(St)_3$ with HSt in TCA. Bottom: ^{13}C NMR spectrum of the final organic product after the thermal decomposition of $Fe(St)_3$ in neat HSt.

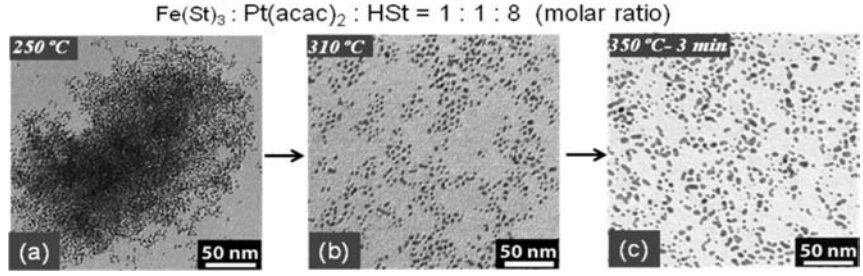

Figure 6. Temporal evolution of the morphology of the Pt (a) and FePt alloy nanocrystals (b and c).

The function of fatty amine as the necessary cosurfactant for the formation of high quality FePt alloy nanocrystals was identified. FePt alloy nanocrystals can be synthesized without the addition of any fatty amine, i.e., just with $Pt(acac)_2$, $Fe(St)_3$, and HSt in a hydrocarbon solvent such as TCA (Figure 6). Different from the typical reaction shown in Figure 4, when the temperature was above ~200 °C, the reaction mixture became turbid gradually. As the reaction temperature further increased to about 310 °C for ~10 min, the solution became optically clear again. At a temperature higher than 310 °C, the heating time for the system to become clear was shortened as the temperature increased.

A control experiment without $Fe(St)_3$ was performed. Similar to the reaction described above, the system became turbid at a similar temperature. However, further heating did not make the system clear. This suggests that Pt nanocrystals could not be stabilized by fatty acids, which is reasonable because fatty acid ligands are very hard Lewis bases and Pt is a very soft Lewis acid. In the reaction described in the above paragraph, the particles became soluble at a temperature higher than 310 °C

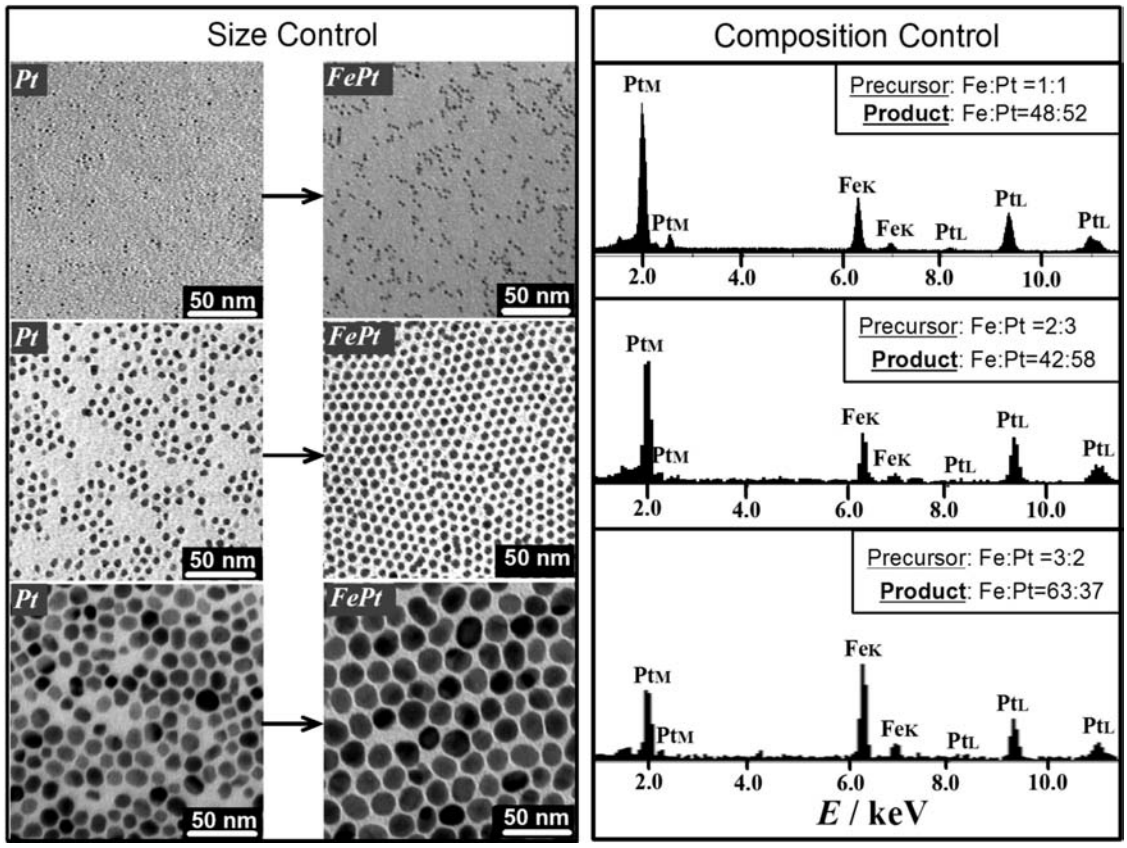

Figure 7. Left column: TEM images of Pt and corresponding FePt nanocrystals with different sizes. Right column: The Fe to Pt ratio (Fe/Pt) determined by EDS in alloy nanocrystals formed with different Fe to Pt precursor molar ratios.

because of the incorporation of iron atoms into the originally formed pure Pt nanocrystals. As a result, the surface Fe atoms on the alloy nanocrystals provided the bonding sites for carboxylate groups. Consistent with this hypothesis, Pt nanocrystals were detected at the relatively low temperatures (Figure 6a). Instead of being isolated, these Pt nanocrystals were clumped together, even with a high dilution. As the reaction temperature increased to above 310 °C, FePt alloy nanocrystals formed and these alloy nanocrystals were found to be isolated (Figure 6b and c). Because of the aggregation of the preformed Pt nanocrystals, the morphology of the FePt nanocrystals formed without amine as the coligands was usually not as round as those formed with some fatty amines added (see Figure 4 as comparison).

It should be pointed out that, as a cosurfactant, the amount of fatty amines added into the reaction system must be reasonably small. If an excessive amount of amines was in place, formation of iron oxide phase(s) became inevitable. One such reaction is provided in the Supporting Information as an example (Figure S9).

Composition and size control can be achieved using the synthetic scheme presented in Figure 1. Because the Fe/Pt ratio is of critical importance in determining the magnetic properties of the nanocrystals, especially after converting to *fct* (face-centered tetragonal) structure for high performance magnets,[42,43] we carried out a systematic study for controlling the Fe/Pt ratio of the resulting nanocrystals.

The Fe/Pt ratio could be varied by changing the precursor ratio (Figure 7, right). In general, the Fe/Pt ratio in the resulting nanocrystals increased monotonically as the Fe/Pt precursor ratio increased, which is qualitatively consistent with the literature on the synthesis of FePt alloy nanocrystals using $Fe(CO)_5$ as the precursor.[21] The reaction temperature, the solution composition, and heating time at the final temperature were all identified as key factors in determining the Fe/Pt atom ratio in the resulting nanocrystals. For example, in a reaction with a sufficient amount of acid, when the temperature was lower than 310 °C, $Fe(St)_3$ decomposed slowly and only a small amount of Fe atoms could be incorporated into the alloy if the reaction time was not sufficiently long. If the amount of fatty acid was not sufficient, some of $Fe(St)_3$ would be converted to FeO_x and the Fe content in the resulting alloy nanocrystals would be low even with prolongated heating. A detailed summary on the Fe/Pt ratio under different reaction conditions is provided as Supporting Information (Table S2).

The size of the final FePt alloy nanocrystals was mainly determined by the size of the Pt nanocrystals and the composition (Figure 7, left panel). As discussed above, Pt nanocrystals always formed at relatively low reaction temperatures and acted as the templates for the resulting alloy nanocrystals. Thus, the volume increase seen in Figure 7 (left panel) would be a result of the incorporation of Fe atoms into the original Pt nanocrystals. Experimentally, this was confirmed by comparing the volume ratio between the original Pt dots and the final FePt dots using the TEM images in Figure 7 (left panel) and the Fe/Pt ratio of the alloy nanocrystals determined by the EDX (Figure S10). The results in Figure S10 further confirmed that the size

(42) Fredriksson, P.; Sundman, B. *CALPHAD: Comput. Coupling Phase Diagrams Thermochem.* **2001**, *25*, 535–548.
(43) Nguyen, H. L.; Howard, L. E. M.; Stinton, G. W.; Giblin, S. R.; Tanner, B. K.; Terry, I.; Hughes, A. K.; Ross, I. M.; Serres, A.; Evans, J. S. O. *Chem. Mater.* **2006**, *18*, 6414–6424.

distribution of the nanocrystals was retained when Fe was incorporated into the Pt seeds.

Discussions

Alloy formation cannot be simply proven by the crystal structure in this specific system because pure Pt metal and FePt alloys can have the same *fcc* crystal structure with very similar lattice parameters. However, these two phases can be distinguished by magnetic measurements (Figure 3 bottom), the composition measurements (Figures 4 and 7), and chemical properties of the resulting nanocrystals.

There might be a slight chance that the magnetic properties and two-element composition discussed in the above paragraph were caused by a core/shell structure. However, this explanation was found to be inconsistent with TEM measurements and chemical properties of the resulting nanocrystals. Because of the dramatic electron density difference, pure Pt and FePt alloy phases can be distinguished readily from pure Fe metal and FeO_x phases by their contrast (Figure S11). In Figure S11, we synthesized core/shell dots and dimers with a distinguishable contrast in the current system when an extremely small Fe/Pt precursor ratio was used, such as Fe/Pt equals 100:1. It was difficult to exactly identify the composition of the core, for either Pt or FePt nanocrystals. The shell (or the larger side of a dimer) with light contrast was found to be a mixture of pure Fe and FeO_x.

Formation of alloy nanocrystals, instead of core/shell ones, was also consistent with the chemical properties of the resulting nanocrystals. The FeO_x and Fe nanocrystals were found to be not stable in acidic conditions, even if it was mildly acidic (pH < 2).[44] However, the nanocrystals claimed to be FePt alloy nanocrystals in this report were stable in 3 mol/L of HCl, which is consistent with the expected stability of the FePt alloy. This means that the surface of the nanocrystals could not be either pure Fe or FeO_x. The surfaces of the final nanocrystals were not pure Pt either because pure Pt nanocrystals were found to be unstable without fatty amines in the system but the so-claimed alloy nanocrystals were stable without fatty amines (see Figure 6 and the related text).

Fatty acids as the alloy mediator can be illustrated by Scheme 1. Fatty acids as the ligands for Fe^{3+} ions and the surface ligands of the resulting nanocrystals were well-known. For the formation of alloy nanocrystals, a critical factor is to eliminate the formation of iron oxide and pure Fe nanocrystals that are accessible under the typical synthetic conditions in the current system. This might not be so critical, however, for the synthetic schemes using $Fe(CO)_5$ as the precursors because the iron is in its zero valence in the precursor and the precursor can decompose at a temperature lower or similar to that of the Pt precursors.

When iron oxide was formed in the current system, the existence of free fatty acids would dissolve the oxide immediately under elevated temperatures (the top arm in Scheme 1). If a large excess of free fatty acids were in place, the dissolution was so rapid that one could assume that the iron oxide phases were not in existence in the system. In this sense, fatty acids were the prohibiting reagents for the formation of iron oxides as observed in some other oxide nanocrystals systems.[45]

Scheme 1. Fatty Acids (Hst As an Example) As the Alloy Mediator[a]

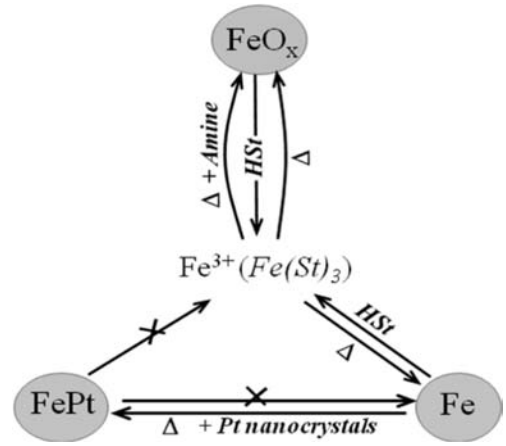

[a] Top arm: formation of iron oxide through either hydrolysis or aminolysis and dissolution of the oxides by HSt. Right arm: reductive formation of Fe^0 and dissolution of Fe^0 back to $Fe(St)_3$ by HSt. Left arm: no direct conversion between $Fe(St)_3$ and FePt nanocrystals. Bottom path: irreversible "sinking" of iron in the form of atomic Fe^0 into Pt nanocrystals to form FePt nanocrystals.

Formation of Fe metal (the right arm in Scheme 1) was essential for the formation of FePt alloy nanocrystals. In the current system, the reducing reagent was identified as the fatty acids and their carboxylate form (Figure 5). From the existence of alkane/alkene, ketone, water, and CO_2 major and minor products, main reactions involved in Fe reduction could be speculated as follows:

$$(CH_3{-}(CH_2)_{16}{-}COO)_3Fe \rightarrow Fe^0 + CO_2 + CH_3{-}(CH_2)_{15}{-}CH_2\bullet \quad (1)$$

$$Fe(St)_3 + HSt \rightarrow Fe^0 + CH_3{-}(CH_2)_{16}{-}CO{-}(CH_2)_{16}{-}CH_3 + HO\bullet + CO_2 \quad (2)$$

$$CH_3{-}(CH_2)_{15}{-}CH_2\bullet + HO\bullet \rightarrow CH_3{-}(CH_2)_{14}{-}CH{=}CH_2 \text{ (or } {-}CH{=}CH{-} \text{ type)} + H_2O \quad (3)$$

The hydrocarbon and hydroxyl radicals were not detected directly, but these hypothetic side products were very consistent with the formation of alkene, alkane, and water. Especially, without the formation of radicals, it would be difficult to imagine the formation of an alkane through combination of two hydrocarbon radicals (reaction not shown) and a $-CH{=}CH-$ type of alkene. Theoretically, one could assume the ketone, CO_2, and water were formed by the decomposition of two molecules of pure HSt. However, this assumption was not consistent with the fact that neat HSt was found to be stable up to 350 °C in a control experiment.

Formation of Fe^0, however, does not guarantee the formation FePt alloy nanocrystals. This is so because the pure iron phase is also a stable phase as reported in literature.[53,54] Thus, an excess amount of free fatty acids was again needed to destroy such iron metal immediately (the product in the right arm in Scheme 1), presumably in the form of nanocrystals as well.

After eliminating the formation of iron oxide and pure iron nanocrystals by free fatty acids (the products in the top and right arms in Scheme 1), the third type of solid state phase, FePt nanocrystals, became the only choice. It occurred supposedly in two steps. In the first, the iron precursor must be reduced

(44) Kim, M.; Chen, Y. F.; Liu, Y. C.; Peng, X. G *Adv. Mater.* **2005**, *17*, 1429-+.
(45) Chen, Y. F.; Kim, M.; Lian, G.; Johnson, M. B.; Peng, X. G. *J. Am. Chem. Soc.* **2005**, *127*, 13331–13337.

to Fe^0 first through the pathway in the right arm in Scheme 1. Competing with the free acids that converted Fe^0 back to the precursor, the Pt nanocrystals preformed at a lower reaction temperature would incorporate Fe^0 into its lattice to form FePt alloy nanocrystals. No matter what the rates for these two competitive reactions were, the alloy nanocrystals would eventually be the final products if the total amount of iron would not exceed its solubility in Pt nanocrystals. This is so because fatty acids could not dissolve iron away from the FePt alloy nanocrystals as discussed above.

Overall, the above discussion indicates that the existence of a large excess of fatty acids made the Pt nanocrystals as the iron sinks to generate FePt alloy nanocrystals. In this sense, fatty acids acted as the alloy mediator in the current system. Without the multirole nature of fatty acids, the formation of high quality FePt nanocrystals in this relatively simple synthetic system without the complication of other solid phases would be difficult to imagine.

Conclusions

In summary, a "greener" method based on air-stable and generic chemicals has been developed to synthesize FePt nanoparticels with controllable size and morphology. Fatty acids, HSt as an example, and the carboxylate form acted as both the reductants and alloying mediators in the synthetic routes. As the alloying mediators, fatty acids set FePt alloy nanocrystals as the trap for Fe^0. The alloy nanocrystals were formed in a two-step fashion, and small amounts of amine were found to be necessary to stabilize the product of the first step, i.e., pure Pt nanocrystals initially formed at a relatively low reaction temperature. As a consequence, the size and composition of the FePt nanocrystals were well controlled by tuning the corresponding size of Pt seeds, the starting ratio of precursors, and the reaction time. These results not only help to understand the formation process of the alloy nanocrystals but also shed further light on the formation of transition metal oxide and semiconductor nanocrystals using the fatty acid/amine ligand system.

Experimental Section

Chemicals. 1-Octadecylamine (ODA, 98%), 1-octadecene (ODE, 90%), *n*-octadecane (90%), *n*-tetracosane (TCA, 99%), platinum(II) acetylacetonate ($Pt(acac)_2$), iron(III) chloride hexahydrate ($FeCl_3 \cdot 6H_2O$), iron(III) nitrate nonahydrate ($Fe(NO_3)_3 \cdot 9H_2O$ were purchased from Alfa. Iron(III) acetylacetonate ($Fe(acac)_3$) was purchased from Aldrich. Stearic acid (HSt, > 97%) was purchased from Fluka. Iron(III) stearate $Fe(St)_3$ was synthesized by using a similar procedure as Mn myristate.[41]

Decomposition Process of $Fe(St)_3$. Typically, 0.315 g (0.35 mmol) of $Fe(St)_3$ and 3.05 g of TCA (9.0 mmol) were loaded in a 25 mL three-necked flask. The mixture was degassed at 120 °C for 10 min. The reaction was maintained at varying temperatures such as 150, 205, 260, and, 305 °C for 5 min. The temperature was then raised to 340 °C. The reaction was monitored by taking aliquots for FT-IR and TEM analysis. The same reaction was also carried out without any TCA, and the gas phase products in the reaction was detected with a clear $Ba(OH)_2$ aqueous solution, which is sensitive to CO_2. The $Ba(OH)_2$ solution remained clear below 200 °C and became slightly turbid at ~220 °C. The $Ba(OH)_2$ solution was significantly more turbid above 300 °C. For gas phase IR measurements, 25 mL of headspace gas was taken by syringe at 150, 205, 260, and 305 °C and at different time intervals at 350 °C. The organic components in the final product were separated by extraction and centrifugation and prepared for NMR and IR characterization. For decomposition of $Fe(St)_3$ in TCA with acid, $Fe(St)_3$ (0.3 mmol), 0.68 g of HSt (2.4mmol), and 2.8 g of TCA were loaded in a 25 mL three-necked flask.

Decomposition Process of $Pt(acac)_2$. $Pt(acac)_2$ (0.3 mmol), HSt (0.9 mmol), and 3.0 g of octadecane were loaded in a 25 mL three-necked flask. The mixture was degassed at 110 °C for 10 min. Then the mixture was heated to 300 °C with a ramping rate of 10 K/min. The mixture formed a clear light yellow solution at 120 °C and began to turn black at ~170 °C. The system heated up to 300 °C. The reaction was monitored by taking aliquots for FT-IR and TEM analysis. The decomposition behavior of $Pt(acac)_2$ in the absence of HSt was also carried using the same procedure above.

Synthesis of Monodisperse FePt Nanocrystals with Size Ranges from 1.8 to 6 nm. In a typical procedure, $Fe(St)_3$ (0.3 mmol), $Pt(acac)_2$ (0.3mmol), 0.69 g of HSt (2.4 mmol), 0.4 g of ODA (1.5 mmol), and 2.8 g of TCA were loaded in a 25 mL three-necked flask. The mixture was degassed at 120 °C for 10 min. Then the system was heated to 350 °C with a ramping rate of 10 K/min and maintained at this temperature for a few hours. The reaction mixture slowly turned deep brown over 180 °C and became completely black at 240 °C. The reaction was monitored by taking aliquots for FT-IR and TEM analysis at different temperatures up to 350 °C and also different reaction intervals at 350 °C. FePt nanocrystals smaller than 2 nm were obtained at the beginning of 350 °C. Increasing the precursor concentrations will lead to 2.5 nm FePt nanocrystals. Decomposition of 0.15 mmol of $Fe(St)_3$, 0.15 mmol of $Pt(acac)_2$ in 0.9 mmol of HSt, and 7.5 mmol of ODA at 330−350 °C for 10 min led to the formation of 3.8 nm nanocrystals. While heating $Fe(St)_3$, $Pt(acac)_2$, HSt, and ODA with a molar ratio of 0.6: 0.6:3.6:25 yields 5.1 nm FePt nanocrystals.

Synthesis of Monodisperse FePt Nanocrystals over 6 nm. In this procedure, ODA acted as both the ligands and the solvent. For example, treating 1.1 mmol of $Fe(NO_3)_3 \cdot 9H_2O$, 1.1 mmol of $Pt(acac)_2$, and 12.5 mmol of ODA at 340 °C for 30 min gave 11 nm FePt fine dots. Decomposition of 0.3 mmol of $Fe(NO_3)_3 \cdot 9H_2O$ as well as $Pt(acac)_2$ in 14 mmol of ODA led to the formation of 7.0 nm FePt nanocrystals. It should be noted that $Fe(NO)_3$ also could be replaced by $Fe(acac)_3$ or $FeCl_3 \cdot 6H_2O$.

Fourier Transform Infrared Spectroscopy (FTIR). FTIR spectra were obtained on a Bruker TGA-FT-IR spectrophotometer by directly spotting hot aliquots onto a CaF_2 salt plate. The temporal concentrations of precursors and ligands were calculated from the integrated peak area of the corresponding peaks. The methyl group ($-CH_3$) peak at 1375 cm^{-1} was chosen as the reference peak for peak area calculations. The gas phase IR was detected using an external gas cell and detector.

Transmission Electron Microscopy (TEM). TEM and high resolution TEM images were taken on a JEOL X-100 at 100 kV using a Formvar coated copper grid and Tecnai F30 field emission gun scanning transmission electron microscope, respectively, using carbon-coated Cu grids. Selected area diffraction (SAED) was taken with a camera length of 76 cm.

Other Characterization Techniques. X-ray energy-dispersive spectroscopy (EDS) was mainly investigated under a Philips ESEM XL30 scanning electron microscope equipped with a field emission gun and operated at 10 kV. X-ray powder diffraction patterns were obtained on a Philips PW1830 X-ray powder diffractometer using a Cu Kα line ($\lambda = 1.5418$ Å). NMR measurements were all carried out on a Bruker 300 MHz instrument. Magnetic properties in Figure 3 were measured using the magnetic susceptibility balance (Johnson Matthey Fabricated Equipment). The FePt nanocrystals were dissolved in toluene as magnetic samples. The concentration was determined by atomic absorption spectroscopy. The magnetic field applied on the samples was 4500 Oe.

Acknowledgment. Financial support from the National Science Foundation is acknowledged.

Supporting Information Available: TGA, FTIR, and NMR results and TEM images as mentioned in the text. This information is available free of charge via the Internet at http://pubs.acs.org.

JA900202T